Health Condition Assessment for Pumped Storage Units Using Multihead Self-Attentive Mechanism and Improved Radar Chart

Xiaoyuan Zhang, Yajun Jiang, Xian-Bo Wang, *Member, IEEE*, Chaoshun Li, *Member, IEEE*, and Jinhao Zhang

亮点：
智能健康评估，异构传感器指标融合
融合问题

***Abstract*—A novel health assessment method for pumped storage units (PSUs) is presented in this article. First, multihead self-attentive mechanism (MSM) combined with quantile regression neural network (QRNN) are proposed to establish a health benchmark model for PSUs to reveal the intricate relationship between the vibration and its multiple influencing factors. Especially, MSM automatically learns the complex interaction features among multiple influencing factors, while QRNN explores the upper bounds of health vibration under specific operational parameters. Then, a fuzzy dimensionless function is constructed to map the deviation of the currently measured vibration from the predicted health vibration to the performance degradation indexes. Finally, an improved radar chart method is proposed to visually illustrate the health condition of multiple measurement locations and give comprehensive health assessment for PSUs. The proposed method is applied in a PSU in Zhejiang province of China. The results of comparative experiments illustrate its effectiveness and feasibility.**

***Index Terms*—Fuzzy dimensionless function (FDF), health condition assessment (HCA), improved radar chart (IRC), multihead self-attentive mechanism (MSM), pumped storage units (PSUs).**

I. Introduction

UNDER the background that China's efforts to achieve the goal of peak carbon dioxide emissions before 2030 and then its carbon neutrality before 2060 [1], the penetration of renewables has been increasing. To balance the renewables, pumped storage units (PSUs) are required to switch frequently and rapidly between a variety of operating modes, such as pumping mode, generating mode, startup mode, shutdown mode, [2] etc. Heavy regulation tasks, variable operating conditions, and harsh operating environments result in increasingly prominent structural fatigue and deterioration of PSUs. If it is not timely addressed, the stability and security of PSUs will eventually be compromised, even the security of their interconnected power systems. Therefore, it is significant to monitor the running condition and carry out health condition assessment (HCA) for PSUs, through which rational maintenance plans can be made to eliminate latent faults in the bud [3], [4].

Many scholars have carried out meaningful explorations to prevent incipient defects of hydroelectric generating units (HGUs). Anomaly detection is one type of commonly used method. For example, Zhu *et al.* [5] proposed a fault detection model for HGUs based on the kernel-independent component analysis and the principal component analysis (PCA). De Santis *et al.* [6] used extended isolation forests to carry out fault detection for a small HGU based on one-year operating data. Ehya *et al.* [7] evaluated several commonly used signal processing tools for fault detection of HGUs operating in noisy environments. Anomaly detection methods enable unsupervised detection of operational anomalies of PSUs based on the characteristics of the monitoring data themselves. However, the performance degradation index (PDI) is not extracted. Thus, it cannot quantitatively assess the health degradation degree.

Building a suitable PDI or health indicator (HI) that can measure the health condition is the general tactic for HCA of complex equipment [8]–[10], which has always been a hot research topic for other equipment, such as lithium-ion batteries [11]–[13], rolling element bearings [9], [14], and aircraft engines [15], [16]. The existing PDI construction methods can be classified into following three categories [17].

1) PDIs based on statistical and signal processing methods [18], [19].
2) PDIs based on data fusion methods [17].
3) PDIs based on machine learning methods [10], [20], [21].

In general, the basic idea of PDI construction is to build an index based on the condition monitoring data to quantify

Manuscript received 10 October 2021; revised 7 February 2022 and 16 March 2022; accepted 31 March 2022. Date of publication 7 April 2022; date of current version 9 September 2022. This work was supported in part by the National Natural Science Foundation of China under Grant 51409095 and in part by the Cultivation Programme for Young Backbone Teachers in Henan University of Technology under Grant 21420171. Paper no. TII-21-4422. *(Corresponding authors: Xiaoyuan Zhang; Chaoshun Li.)*

Xiaoyuan Zhang, Yajun Jiang, Xian-Bo Wang, and Jinhao Zhang are with the College of Electrical Engineering, Henan University of Technology, Zhengzhou 450001, China (e-mail: freedon@haut.edu.cn; 1765115322@qq.com; xb_wang@live.com; 1975344306@qq.con).

Chaoshun Li is with the School of Civil and Hydraulic Engineering, Huazhong University of Science and Technology, Wuhan 430074, China (e-mail: csli@hust.edu.cn).

Color versions of one or more figures in this article are available at https://doi.org/10.1109/TII.2022.3165642.

Digital Object Identifier 10.1109/TII.2022.3165642

the deviation of the current operating state from the desired health operating state of the equipment. Recently, due to the powerful ability of nonlinear expression and automatic feature extraction, deep learning-based PDIs have been proposed. For example, Ye and Yu [20] used long short-term memory convolutional autoencoder combined with multivariate Gaussian distribution (LSTMCAE-MGD) to measure the deviation of degradation sample from the health space, based on which an HI was generated to carry out HCA for aircraft engines. Guo *et al.* [22] built a multiscale convolutional autoencoder network to learn features from the sensor signals. The relative similarity of learned features between the baseline sample data and the currently acquired sample data is calculated as an HI. Although many state-of-the-art methods have been developed for HCA of different complex equipment, there exist following two critical shortcomings when used in PSUs.

1) Most existing PDI modeling methods directly learn PDIs from the performance parameters, usually vibration signals, while the influencing factors of different working conditions are rarely considered, which is not suitable for PSUs. Because PSUs have complex and variable operating conditions, the health vibration varies greatly under different operating conditions.
2) The entire lifetime "run-to-failure" data are required for most PDI methods, which are almost impossible to be obtained for PSUs with long life, expensive value, and complex structure.

A viable option is to establish a health benchmark model (HBM)-based PDI for PSUs. The HBM is established as the complex relationship of working condition parameters and the performance parameters when PSUs work in good conditions. The online operating condition parameters are input into the established HBM to predict the corresponding performance parameters. The deviation of the measured performance parameters from the predicted performance parameters is defined as the PDI to assess the current health condition. Based on this idea, An *et al.* [3], [23] had made useful attempts for HCA of HGUs. They selected the active power and the water head as the condition parameters and the upper bracket horizontal vibration, as performance parameter to construct the HBM for HGUs. The relative deviation (RD) between the online measured vibration and the health vibration predicted by HBM is defined as the PDI. These efforts provide an option for HCA of PSUs. However, there still exist the following limitations.

1) The existing HBM is not comprehensive, as it only considered one sensor vibration signal and two influencing factors. Since each sensor signal contains incomplete information about the complex degradation process, effective methods are needed to extract complete and valuable information from multiple sensors [21]. In addition, only considering two influencing factors of vibration is insufficient, as the vibration of PSUs is influenced by many factors, such as hydraulic, mechanical, electromagnetic, and so on.
2) The regression model used in the current HBM, such as radial basis function interpolation [3], Shepard surface [23], and backpropagation neural network (BPNN) [4], cannot well reveal the complex interactive relationship between multiple influencing factors. In addition, the prediction results of the existing HBM are fixed points, the uncertainty information existing in the vibration is not fully considered.
3) The current methods directly use the RD between the measured vibration and the predicted health vibration as the PDI, which has great randomness and may not be able to fully reflect the actual operation of the PSU. Recently, Shan *et al.* [4] added guide vane opening as another condition parameter to the influencing factors of vibration and used BPNN to construct the HBM for PSUs. However, the limitations have not been thoroughly broken through.

Inspired and motivated by the abovementioned facts, a novel HCA framework for PSUs is proposed in this article, which focuses on the following three aspects to fill the knowledge gaps in previous research.

1) A more comprehensive HBM is established, using the complex relationship of multiple sensor vibration signals collected from four measurement locations of the shaft and their seven influencing factors. Inspired by the remarkable performance in modeling complicated relations [24], [25], a multihead self-attentive mechanism (MSM) is extended to automatically learn the complex interactive relationship among multiple influencing factors. In addition, to quantify the uncertainty information of the vibration, a quantile regression neural network (QRNN) [26] is used to predict the upper bounds of the health vibration under specific operating parameters. The proposed HBM is called MSM-QRNN.
2) A novel PDI modeling method is proposed for PSUs under the situation without "run-to-failure" data. By analyzing the distribution characteristics of historical vibration and warning values specified by the regulations, two PDI thresholds corresponding to early degradation and abnormal operation are determined, respectively. A nonlinear fuzzy dimensionless function (FDF) is constructed to map the deviation of currently measured vibration from the predicted health vibration to the PDI.
3) A comprehensive health assessment method based on multisensor vibration signals is proposed. Considering that the field operators need to grasp the health conditions of the PSU reflected by multiple sensors in a real-time, dynamic, and intuitive manner, an improved radar chart (IRC) method is proposed to intuitively, dynamically, and comprehensively assess the health status of PSUs.

The proposed HCA method is applied in a PSU located in Zhejiang province of China to verify its feasibility and effectiveness. The rest of this article is organized as follows. Section II introduces the overall framework of the proposed method. Section III gives the proposed HBM. The comprehensive assessment model is presented in Section IV. Section V gives the experimental verification and comparison studies to evaluate the performance of the proposed method. Finally, Section VI concludes this article.

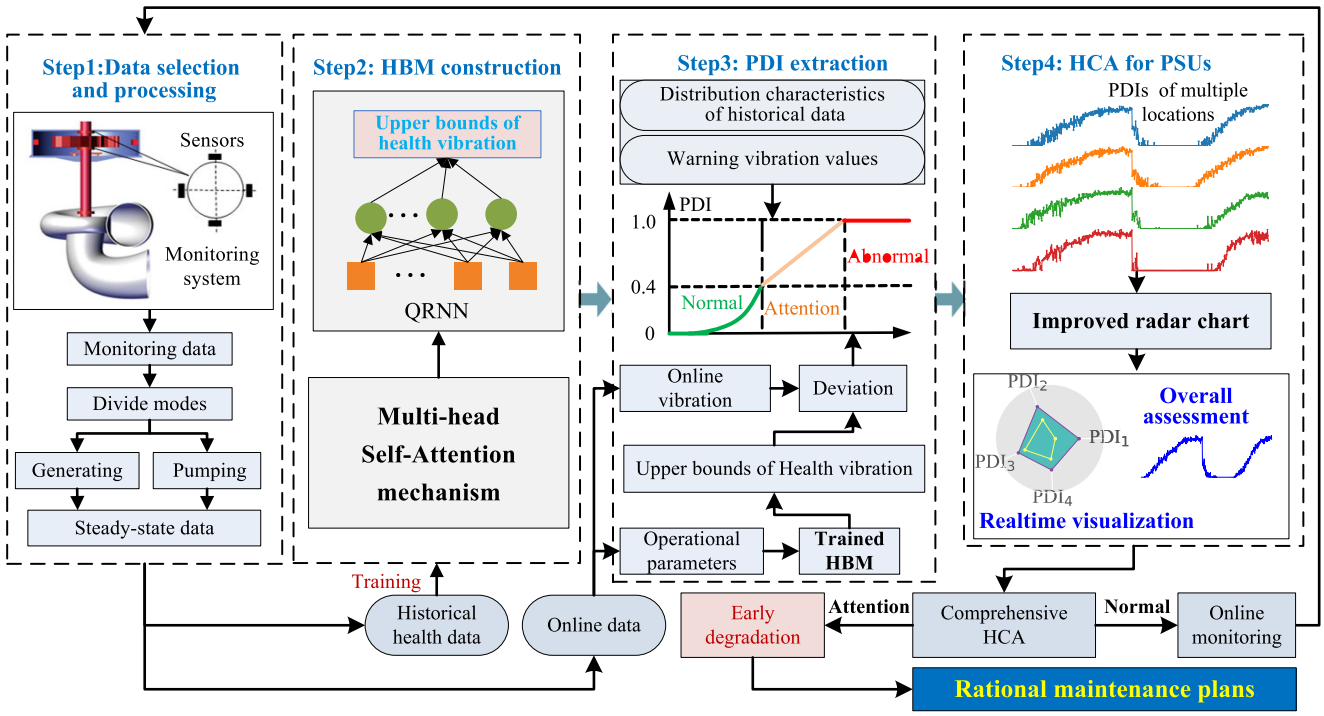

Fig. 1. Overall framework of the proposed HCA method.

II. Overall Framework of the Proposed Method

The overall framework of the proposed HCA method is shown in Fig. 1. It mainly includes four steps: 1) data selection and processing; 2) HBM construction; 3) PDI extraction; and 4) HCA for PSUs.

A. Step 1: Data Selection and Processing

To avoid the influence of noise in the process of start and stop of PSUs, the monitoring data collected from 1 h after the start-up to 10 min before the shutdown are selected as steady-state data. Each operation between start-up and shutdown is considered as an assessment unit. The root mean square (rms) value is used to represent the overall vibration condition for each time of operation. The HCA is carried out under the generating mode and the pumping mode, respectively.

B. Step 2: HBM Construction

The data collected during the initial period after the overhaul are selected as the health dataset. The working condition parameters, which are water head H, active power P, reactive power Q, excitation current I, excitation voltage U, and the highest temperature of the oil outlet of the upper and lower guide bearings, $T1$ and $T2$, respectively, are selected as input. The vibration signals collected from four sensors located at X-direction of upper guide bearing (upper X), Y-direction of upper guide bearing (upper Y), X-direction of lower guide bearing (lower X), and Y-direction of lower guide bearing lower Y (lower Y), (U_x, U_y, L_x, L_y), are selected as output to train the MSM-QRNN model. The trained MSM-QRNN is selected as the HBM.

C. Step 3: PDI Extraction

The online monitoring operating parameters are input into the HBM to get their corresponding upper bounds of health vibration. The distribution characteristics of historical vibration data and the warning vibration values given by the power station are used to determine two PDI thresholds corresponding to early degradation and abnormal operation. With the help of the thresholds, a nonlinear FDF is constructed to map the deviation of the measured vibration from the predicted health vibration to the PDI.

D. Step 4: HCA for PSUs

Based on the obtained PDIs, the IRC is used to visualize the degree of real-time degradation of different measurement locations, also give a comprehensive health assessment of the PSU. According to the comprehensive PDI value, the operational personnel can determine whether the PSU is operating in the normal zone or the attention zone of early degradation. If it is running in the attention zone, an early warning will be given; also a rational maintenance plan can be made. If the PSU is running in the normal zone, it will go back to step 1 and continue the abovementioned steps 1–4.

III. HBM Based on MSM-QRNN

The HBM is essentially a regression model that uses vibration collected from multiple sensors as response variables and multiple influencing factors as explanatory variables. The structure of the proposed HBM is shown in Fig. 2, which includes feature

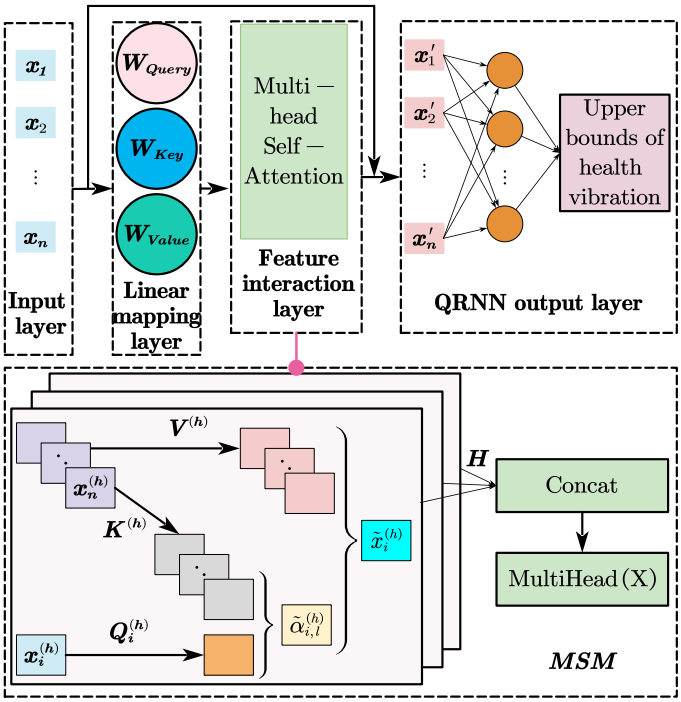

Fig. 2. Proposed MSM-QRNN-based HBM.

input layer, linear mapping layer, MSM feature interaction layer, and QRNN output layer.

A. Input Layer and Linear Mapping Layer

As shown in Fig. 2, $\boldsymbol{x}_1, \boldsymbol{x}_2, \ldots, \boldsymbol{x}_n$ are the input features representing n influencing factors of vibration. Let $\boldsymbol{X} = [\boldsymbol{x}_1, \boldsymbol{x}_2, \ldots, \boldsymbol{x}_n]$ be the input matrix, where $\boldsymbol{X} \in \boldsymbol{R}^{m\times n}$, m is the number of observed points. In the linear mapping layer, $\mathbf{X}$ is linearly mapped to H groups of feature subspaces, namely H heads: $\{\boldsymbol{Q}^{(h)}, \boldsymbol{K}^{(h)}, \boldsymbol{V}^{(h)}\}$, $h = 1, \ldots, H$, by

$$\boldsymbol{Q}^{(h)} = \boldsymbol{X}\boldsymbol{W}^{(h)}_{\text{Query}}, \boldsymbol{K}^{(h)} = \boldsymbol{X}\boldsymbol{W}^{(h)}_{\text{Key}}, \boldsymbol{V}^{(h)} = \boldsymbol{X}\boldsymbol{W}^{(h)}_{\text{Value}} \quad (1)$$

where $\boldsymbol{W}^{(h)}_{\text{Query}}, \boldsymbol{W}^{(h)}_{\text{Key}}, \boldsymbol{W}^{(h)}_{\text{Value}} \in \boldsymbol{R}^{n\times n'}$ are the transformation matrices that map the raw feature space $\boldsymbol{R}^n$ into a new feature space $\boldsymbol{R}^{n'}$. $\boldsymbol{Q}$, $\boldsymbol{K}$, and $\boldsymbol{V}$ denote the query vector, key vector, and value vector, respectively.

B. MSM Feature Interaction Layer

Recently, the multihead self-attentive network has achieved remarkable performance in calculating correlations over a temporal sequence [25]. It shows superiority for modeling arbitrary word dependency in the natural language processing field [25], [27]. This study extends the self-attentive mechanism to calculate the complicated high-order interaction relations, namely the attention weights, among different raw features. The normalized attention weights times their relevant features are added to form the high-order interaction features. This process is executed in parallel in H subspaces, namely H heads, which are concatenated to form meaningful combinatorial features.

Taking feature $\boldsymbol{x}_i^{(h)}$ $(h = 1, 2, \ldots, H, i = 1, 2, \ldots, n)$ as an example. The new combinatorial high-order interaction feature $\tilde{\boldsymbol{x}}_i^{(h)}$ under a specific attention head h, can be calculated by

$$\tilde{\boldsymbol{x}}_i^{(h)} = \sum_{l=1}^{n} \tilde{\alpha}_{i,l}^{(h)} \boldsymbol{V}_l^{(h)} \quad (2)$$

where $\tilde{\alpha}_{i,l}^{(h)} = \text{soft}\max(\boldsymbol{Q}_i^{(h)} \cdot \boldsymbol{K}_l^{(h)} / \sqrt{d_{q,k}})$ is the normalized self-attention weight calculated by the scaled dot-product attention operation [25] between features $\boldsymbol{x}_i^{(h)}$ and $\boldsymbol{x}_l^{(h)}$, $d_{q,k}$ represents the column number of the matrices $\boldsymbol{Q}_i^{(h)}$ and $\boldsymbol{K}_l^{(h)}$, and $\tilde{\boldsymbol{x}}_i^{(h)}$ represents a new combinatorial feature learned from feature $\boldsymbol{x}_i$ and its relevant features under head h. Through the abovementioned procedure, all interacting features under head h, $\boldsymbol{head}_h$, can be got by

$$\boldsymbol{head}_h = \left[\tilde{\boldsymbol{x}}_1^{(h)}; \tilde{\boldsymbol{x}}_2^{(h)}; \ldots; \tilde{\boldsymbol{x}}_n^{(h)}\right]. \quad (3)$$

However, a feature is also likely to be involved in different combinatorial features. Thus, the interaction features learned in all heads are concatenated by

$$\text{MultiHead}\,(\boldsymbol{X}) = \text{Concat}\,(\boldsymbol{head}_1, \boldsymbol{head}_2, \ldots, \boldsymbol{head}_H)\,\boldsymbol{W}^O \quad (4)$$

where $\boldsymbol{W}^O \in \boldsymbol{R}^{n'H\times n}$ is a projection matrix in the case of dimension mismatching.

To preserve previously learned combinatorial features, standard residual connections are added to the network, which is shown as

$$\boldsymbol{X}' = \text{MultiHead}\,(\boldsymbol{X}) + \boldsymbol{X} \quad (5)$$

where $\boldsymbol{X}' = [\boldsymbol{x}_1', \boldsymbol{x}_2', \ldots, \boldsymbol{x}_n']$ represents the sum of the combined features and the original features.

C. QRNN Output Layer

Originally introduced by Taylor [28], QRNN perfectly reveals the effects of the explanatory variables on the whole conditional distribution of response variables by taking the advantage of quantile regression and artificial neural networks [29]. Especially, it can effectively quantify the uncertainty of the prediction process [30].

In the proposed HBM, QRNN is used to estimate the upper bounds of health vibration of PSUs. As shown in Fig. 2, the aforementioned $\boldsymbol{X}'$ got by the MSM feature interaction layer is input into QRNN, where a single hidden-layer feedforward network is used for nonlinear mapping. Its feedforward output is

$$f\,(\boldsymbol{X}') = \text{ReLU}\,(\boldsymbol{X}'\boldsymbol{W}_1 + \boldsymbol{b}_1)\,\boldsymbol{W}_2 + \boldsymbol{b}_2 \quad (6)$$

where $\text{ReLU}(z) = \max(0, z)$ is a nonlinear activation function, $\boldsymbol{W}_1$ and $\boldsymbol{W}_2$ are the two weight matrices, and $\boldsymbol{b}_1$ and $\boldsymbol{b}_2$ are the bias vectors.

The following loss function is adopted to train the MSM-QRNN:

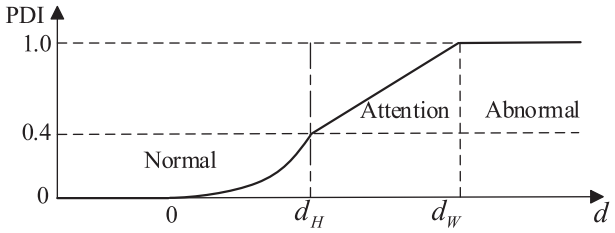

Fig. 3. FDF.

$$\text{Loss} = \sum_{i|y_i \geq f\left(\boldsymbol{X}'_i, \boldsymbol{W}, \boldsymbol{b}\right)} \tau \left| y_i - f\left(\boldsymbol{X}'_i, \boldsymbol{W}, \boldsymbol{b}\right) \right| + \sum_{i|y_i < f\left(\boldsymbol{X}'_i, \boldsymbol{W}, \boldsymbol{b}\right)} (1-\tau) \left| y_i - f\left(\boldsymbol{X}'_i, \boldsymbol{W}, \boldsymbol{b}\right) \right| \quad (7)$$

where $\boldsymbol{X}'_i$ is the input feature that influences the output target y_i, i is the number of samples, and $\tau \in (0, 1)$ denotes the quantile point. $\boldsymbol{W} = \{\boldsymbol{W}_{\text{Query}}, \boldsymbol{W}_{\text{Key}}, \boldsymbol{W}_{\text{Value}}, \boldsymbol{W}^O, \boldsymbol{W}_1, \boldsymbol{W}_2\}$ and $\boldsymbol{b} = \{\boldsymbol{b}_1, \boldsymbol{b}_2\}$ are the parameters to be learned, which can be updated by minimizing (7) using stochastic gradient descent method. In this study, the output of the HBM under $\tau = 0.95$, is considered as the upper bound of the health vibration.

IV. Comprehensive HCA

A. Proposed PDI

After obtaining the trained HBM, the online monitoring operational parameters are input into the trained HBM to predict the upper bounds of the health vibration. The deviation of measured vibration from the upper bound of health vibration is denoted as d, which characterizes the extent to which the current health condition deviates from the ideal health condition. Here, a mathematical model is needed to map d to the PDI, which should be able to well-sense the early degradation of the PSU to prevent failures and make rational maintenance plans. Therefore, it is critical to determine reasonable thresholds to divide the health-status interval of the PSU. However, this is a challenging problem as there are no "run-to-failure" data for PSUs. This study makes full use of the distribution characteristics of historical vibration and warning values specified by the regulations to determine two thresholds to divide the health status of PSUs into three intervals: 1) normal; 2) attention; and 3) abnormal. And, a nonlinear FDF function is constructed to map d to the corresponding PDI intervals. The detailed process is as follows.

First, the historical steady-state data of PSUs are statistically analyzed to obtain the 0.05 quantile $v_{0.05}$ and the 0.95 quantile $v_{0.95}$. And, vibration warning value v_W is obtained by querying the operation regulations of the power station. Then, we define two thresholds: 1) the attention threshold $d_H = v_{0.95} - v_{0.05}$; and 2) the abnormal threshold $d_W = v_W - v_{0.05}$. By using the attention threshold and abnormal threshold, an FDF is constructed by (8). Its corresponding function curve is shown in Fig. 3.

$$\text{PDI}(d) = \begin{cases} 0 & d \leq 0 \\ \left(1 - \frac{d_H - d}{d_H}\right) \cdot e^{\left(\frac{d_H - d}{d_H}\right) \cdot b} \times \rho & 0 < d \leq d_H \\ \frac{d - d_H}{d_W - d_H} \times (1 - \rho) + \rho & d_H < d \leq d_W \\ 1 & d > d_W \end{cases} \quad (8)$$

where b is a shape coefficient. After several tests, b is set as 1. ρ is a preset PDI threshold. If PDI is lower than ρ, the PSU is running in the normal zone. Otherwise, the PSU starts to undergo some degradation. Drawing on the findings of the literature [31], ρ is set as 0.4. It can be easily seen from (8) that the proposed PDI is in a (0, 1) interval. The greater the PDI, the more serious the performance degradation.

B. Comprehensive Assessment Based on IRC

RC is one of the most popular methods for comprehensive performance evaluation, as it can intuitively display the status of the to-be-evaluated object from multiple indicators [32]. However, the traditional RC method has the following shortcomings.

1) If the order of indicators changes, the area and perimeter of the polygon enclosed by the endpoints of different indicators will change, which results in different assessment results.
2) The traditional RC method does not differentiate between indicators with different levels of importance.

It is not suitable for a complex system, such as a PSU, in which different indicators building from different sensors may have different contributions to the degradation behavior. To overcome the abovementioned shortcomings, an IRC method is proposed. It mainly includes the following steps.

1) The PDIs for four measurement locations: a) upper X (PDI_1); b) upper Y (PDI_2); c) lower X (PDI_3); and d) lower Y (PDI_4), are selected as four indicators.
2) PCA is applied to the historical vibration signals collected from four measurement locations to get four weights: a) θ_1; b) θ_2; c) θ_3; and d) θ_4, where $\sum_{i=1}^{4} \theta_i = 1$. According to the weights, a unit circle is divided into four sectors corresponding to: a) PDI_1; b) PDI_2; c) PDI_3; and d) PDI_4, as shown in Fig. 4.
3) The value of PDI_i, $i = 1, 2, 3, 4$, is used to determine the length of the ith angle bisector. Then, the closed polygon in the unit circle is obtained by connecting the endpoints of all angular bisectors in sequence, as shown in Fig. 4.
4) The comprehensive PDI is calculated by

$$\text{PDI}_C = \frac{S + L}{S_1 + L_1} \quad (9)$$

where PDI_C is the result of the comprehensive assessment, S is the area of the closed polygon, L is the perimeter of the closed polygon, and S_1 and L_1 are the area and perimeter of the closed polygon, respectively, when PDI_1, PDI_2, PDI_3, and PDI_4 are all equal to 1.

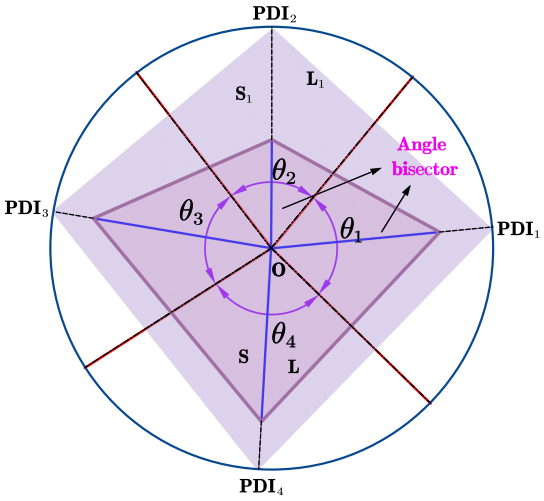

Fig. 4. Schematic of the proposed IRC method.

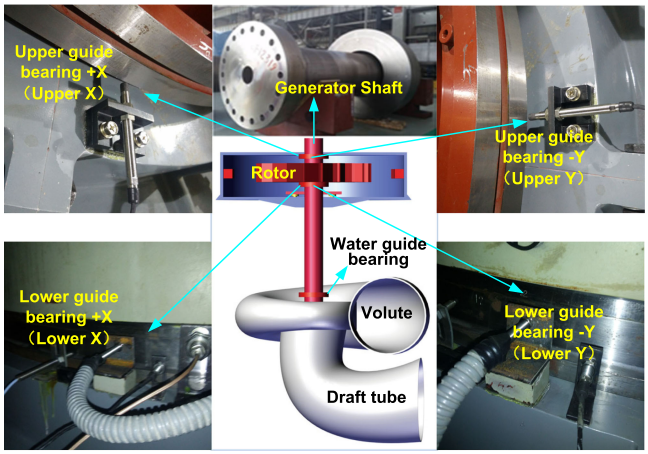

Fig. 5. Structure of the PSU and the location of the sensors.

V. Experimental Results and Comparisons

In this section, the effectiveness and feasibility of the proposed method are evaluated in a PSU located in Zhejiang province of China, which was put into operation on October 31, 2016. The PSU is equipped with a single-stage mixed-flow reversible pump-turbine unit with a capacity of 375 MW. The structure of the PSU and locations of the sensors are shown in Fig. 5. This article focuses on evaluating the health conditions of the generator shaft. The vibration signals collected from upper *X*, upper *Y*, lower *X*, lower *Y* are used as the performance parameters. According to the procedure presented in Section II, the HCA can be carried out. The detailed procedure of how the proposed HCA method works and comprehensive comparison experiments are as follows.

A. Experimental Data and Setup

The monitoring data are collected from January 1, 2019, to August 31, 2020, with a sampling period of 1 min. During this period, the PSU underwent 774-times generating modes and 635-times pumping modes. As described in step 1 of Section II, the HCA is carried out under the generating mode and the pumping mode, respectively. The steady-state data for the generating mode have 88 586 points and that for the pumping mode have 169 443 points. Fig. 6 shows the time-domain waveforms of the vibration at upper *X*, upper *Y*, and lower *X*, lower *Y* from January 1, 2019 0:00 A.M. to January 5, 2019 23:59 P.M., from which we can see that the vibration fluctuates drastically along with the frequent switching of pumping-generating and start–stop of the PSU.

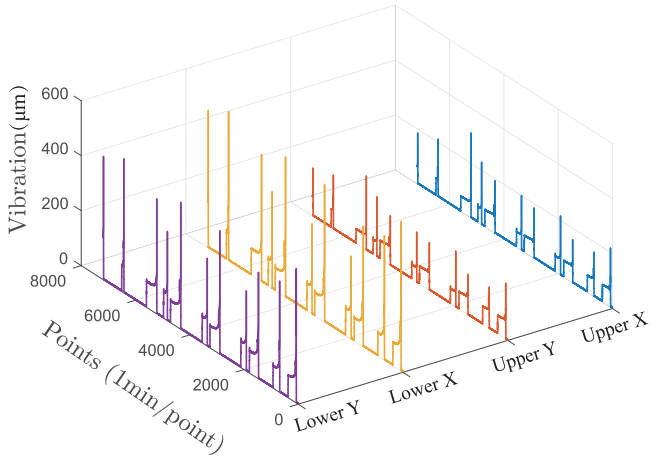

Fig. 6. Vibration of four measurement locations from January 1, 2019, 0:00 A.M. to January 5, 2019, 23:59 P.M., 7200 points.

Generally speaking, the PSU is in a relatively healthy state at the initial stage after the new commissioning or an overhaul. By checking the maintenance records, we know that the PSU underwent one C-Class maintenance from November 7, 2018, to November 29, 2018. Thus, the monitoring data of the first 100 operations of the generating mode and the pumping mode in early 2019 are selected as the health data for these two modes, respectively. The rest data are used to assess the health conditions of the PSU.

The computing platform is a PC with the following features: Intel (R) Core (TM) i7-7700 k CPU @ 3.60 GHz 8 cores, 16 G RAM, a Windows 10 version operating system, Python 3.7 development environment. The number of nodes for the input and output of MSM-QRNN is 7 and 4, respectively. The number of hidden-layer nodes of QRNN is set to be 10 by the trial-and-error method.

B. HBM Construction

For HBM construction, 70% of the health data are randomly selected to form the training set. The working condition parameters: $\{H, P, Q, I, U, T1, T2\}$ and the shaft vibrations: (U_x, U_y, L_x, L_y) in the training dataset are selected as input and output labels, respectively, to train the HBM. The HBM is trained with its parameters, $\boldsymbol{W} = \{\boldsymbol{W}_{\text{Query}}, \boldsymbol{W}_{\text{Key}}, \boldsymbol{W}_{\text{Value}}, \boldsymbol{W}^O, \boldsymbol{W}_1, \boldsymbol{W}_2\}$ and $\boldsymbol{b} = \{\boldsymbol{b}_1, \boldsymbol{b}_2\}$, updated by minimizing (7). The remaining 30% of the health status data are used to test the HBM model.

TABLE I
COMPARISON OF MSM-QRNN AND QRNN FOR DIFFERENT MEASUREMENT LOCATIONS UNDER 95% QUANTILE

Mode	Locations	QRNN		MSM-QRNN	
		PICP	PINAW	PICP	PINAW
Generating	upper X	0.9386	0.1454	0.9567	0.1388
	upper Y	0.9460	0.1572	0.9520	0.1560
	lower X	0.9413	0.1055	0.9503	0.1049
	lower Y	0.9503	0.1193	0.9580	0.1134
Pumping	upper X	0.9520	0.1682	0.9557	0.1613
	upper Y	0.9486	0.1558	0.9560	0.1472
	lower X	0.9520	0.1015	0.9557	0.0961
	lower Y	0.9490	0.1181	0.9560	0.1101

To illustrate the performance of the proposed HBM, some comparative studies are done. First, to illustrate the necessity of MSM in the proposed HBM, MSM-QRNN is compared with QRNN at 95% quantile. Two probabilistic evaluation criteria: 1) the prediction interval coverage probability (PICP); and 2) prediction interval normalized averaged width (PINAW) [30], are employed to evaluate their performance. From the uncertainty prediction point, a smaller PINAW with a higher coverage probability (larger PICP) is preferred. The results are reported in Table I. Moreover, to further evaluate the proposed MSM-QRNN, it is compared with BPNN, which is used to construct HBM for PSUs in [4], and RBFNN, which is used to depict the relationship between battery aging level and its influencing factors in [12]. In addition, as one of the state-of-the-art regression models, support vector regression (SVR) [33] is also selected as a comparison method. To facilitate comparison with BPNN, RBFNN, and SVR, referring to the literature [29], we select the median of the complete probability distribution of predicted vibration as point prediction results of MSM-QRNN. Two deterministic evaluation criteria [29]: 1) mean absolute error (MAE); and 2) rms error (rmse), are employed as the evaluation indicators. The results are reported in Table II.

It can be seen from Table I that the proposed MSM-QRNN yields higher PICP and narrower PINAW than QRNN in all working conditions and all measurement locations. This result shows the necessity of using MSM to learn interaction relationships among multiple influencing factors of vibration. From Table II, we can see that the results of BPNN, RNFNN, and SVR are comparable, and in general, the results of SVR are slightly better, but they are all inferior to the proposed MSM-QRNN. These results demonstrate the outstanding performance of the proposed HBM. As mentioned before, the vibration of PSUs is influenced by various factors, such as hydraulic, mechanical, and electromagnetic, which are interdependent and coupled with each other. Traditional machine learning-based regression models cannot learn the interaction features between multiple influencing factors. In addition, traditional point prediction methods cannot reflect the uncertainty information of the vibration. However, in the proposed MSM-QRNN, the MSM is responsible for learning the complex interaction relationship among the multiple influencing factors, while QRNN predicts the upper bounds vibration of the PSU. It not only can reveal the complex correlation relationships between different influencing factors, but also can quantify the uncertainty information of the vibration.

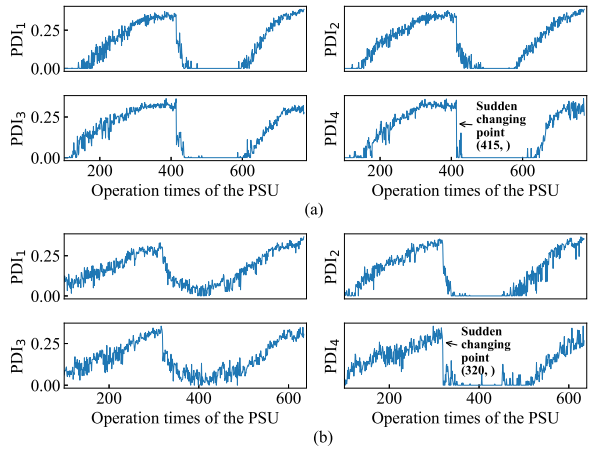

Fig. 7. PDIs for four measurement locations of the PSU: upper X (PDI_1), upper Y (PDI_2), lower X (PDI_3), and lower Y (PDI_4). (a) Generating mode. (b) Pumping mode.

C. PDI Construction

After HBM construction, the PDIs can be extracted according to step 3 of Section II and Section IV-A. The PDI sequences for four measuring locations: 1) upper X (PDI_1); 2) upper Y (PDI_2); 3) lower X (PDI_3); and 4) lower Y (PDI_4), are shown in Fig. 7, from which we can see that all the PDI sequences have a similar overall trend. The PDIs gradually rise with the increase of the cumulative operation times of the PSU. After experiencing a sharp drop (for the generating mode after the 415th operation and for the pumping mode after the 320th operation), they gradually rise again. By checking the operation records, the PSU was out of service for maintenance from October 10, 2019, to November 18, 2019. This period happens to correspond to the time from the 415th start-up to the 416th start-up for the generating mode and from the 320th start-up to the 321st start-up for the pumping mode. Thus, all the PDI sequences are consistent with the operational reality.

To evaluate the advantages of the proposed PDI, it is compared with several state-of-the-art PDI construction methods. As aforementioned, previous research [3], [4], [23] directly used RD between the measured vibration and the predicted health vibration to define PDIs. Thus, first, we construct a comparison method called MSM-QRNN-RD, which uses RD to replace the FDF of our proposed method, to demonstrate the superiority of the proposed FDF. Also, BPNN-RD reported in [4] is used for comparison, which uses the RD between the measured vibration and the health vibration predicted by BPNN-based HBM to define the PDI. Take the PDI sequence of upper X, PDI_1, as an example. The PDI_1 sequences got by the three methods are shown in Fig. 8, from which we can see that all methods can accurately detect the sudden changing point caused by the maintenance. But, BPNN-RD and MSM-QRNN-RD have bigger local fluctuations than the proposed method. Especially, we can see that the PDIs got by BPNN-RD and MSM-QRNN-RD exceed the threshold many times between the 300th and

TABLE II
COMPARATIVE STUDIES BETWEEN THE PROPOSED MSM-BPNN AND SOME PUBLISHED MODELS

Mode	Locations	BPNN [4]		RBFNN [12]		SVR [33]		MSM-QRNN(Median)	
		MAE(%)	RMSE(%)	MAE(%)	RMSE(%)	MAE(%)	RMSE(%)	MAE(%)	RMSE(%)
Generating	upper X	6.90	8.87	6.98	8.87	6.82	8.61	**4.07**	**5.35**
	upper Y	7.04	9.01	7.23	9.16	6.93	8.80	**4.46**	**5.96**
	lower X	6.67	8.30	6.84	8.54	6.85	8.30	**4.28**	**5.92**
	lower Y	7.03	8.69	7.10	8.86	7.04	8.54	**4.78**	**6.50**
Pumping	upper X	8.50	10.91	8.46	10.76	8.39	10.70	**6.27**	**8.11**
	upper Y	8.30	10.76	8.21	10.56	8.24	10.53	**5.67**	**7.49**
	lower X	5.34	6.65	5.19	6.51	5.26	6.50	**3.87**	**4.92**
	lower Y	6.21	7.80	6.05	7.53	6.05	7.46	**4.71**	**6.00**

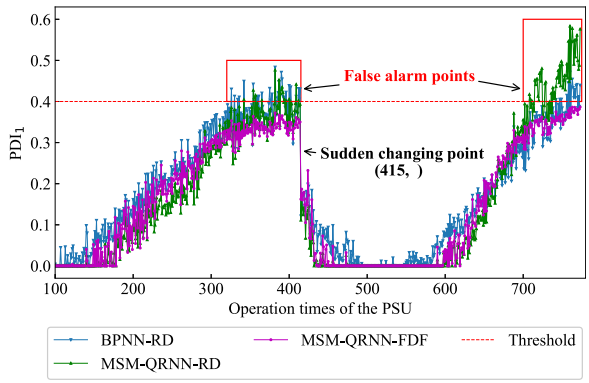

Fig. 8. PDI sequences for the proposed method and two comparison methods.

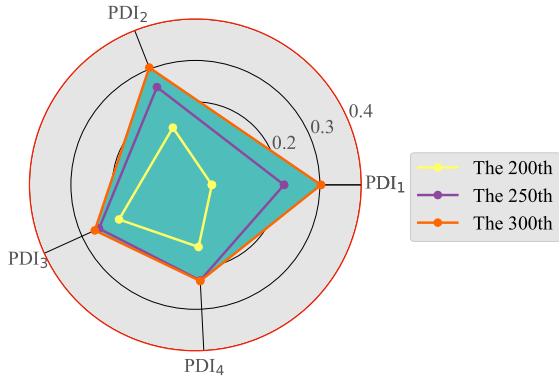

Fig. 9. Example of IRC to dynamically show the health state of the PSU.

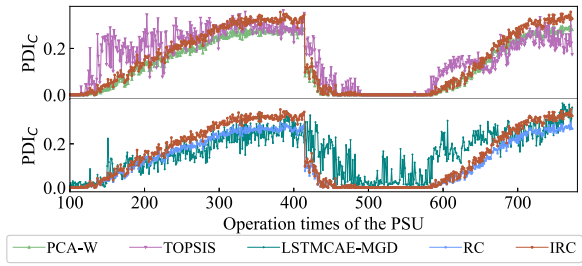

Fig. 10. Comprehensive PDI sequences of the PSU for different methods.

400th operations and after the 700th operation, while the PDIs got by the proposed method never exceed the threshold. By checking the operation and maintenance records, the PSU has never deviated from normal operations from 2019 to 2020. Thus, the proposed method is more in line with the actual operation, as it is more stable and has no false alarm points.

In addition, to further quantitatively evaluate the performance of the proposed PDI, two commonly used metrics for machine HIs are employed [8] as follows.

1) *Monotonicity:*

$$\text{Mon}(X) = \frac{1}{K-1}\left|\text{No. of } d/dx > 0 - \text{No.of } d/dx < 0\right| \tag{10}$$

where $X = \{x_k\}_{k=1:K}$ is the PDI sequence with x_k representing the PDI value at time t_k, K is the total number of the PDI values included in the sequence, $d/dx = x_{k+1} - x_k$ denotes the difference of the PDI sequence, No. of $d/dx > 0$ and No. of $d/dx < 0$ represent the number of the positive differences and the negative differences, respectively. The monotonicity matric measures the absolute difference of the positive and negative derivatives of X. It changes from 0 to 1, and a higher score means better performance in monotonicity.

2) *Robustness:*

$$\text{Rob}(X) = \frac{1}{K}\sum_{k=1}^{K}\exp\left(-\frac{x_k - x_k^T}{x_k}\right) \tag{11}$$

where x_k is the indicator value of X at t_k and x_k^T is the mean trend value of the PDI at t_k. Like monotonicity, robustness is also an inherent property of a PDI itself. It also changes from 0 to 1, and a higher score means better performance in robustness.

According to (10) and (11), the monotonicity and robustness metrics for BPNN-RD, MSM-QRNN-RD, and MSM-QRNN-FDF are orderly calculated as (0.091, 0.233, 0.260) and (0.805, 0.860, 0.880), respectively. Obviously, MSM-QRNN-FDF outperforms the other two methods whether in monotonicity or robustness metric. The reasons can be explained as two aspects as follows.

1) MSM-QRNN is better than BPNN, which has been verified in Section V-B.
2) FDF has better stability than RD in defining PDIs for PSUs, as it fully considers the statistical distribution characteristics of historical vibration data.

D. Comprehensive Health Assessment for PSUs

After obtaining the PDIs for four measurement locations, the IRC and the comprehensive PDI can be got according to the procedure described in Section IV-B. The weights calculated

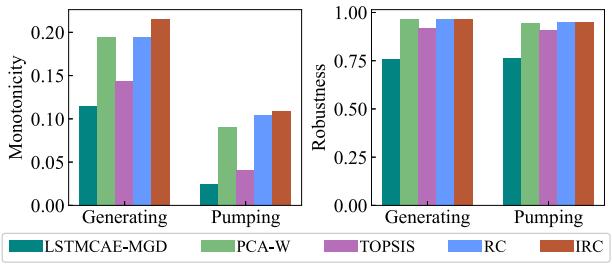

Fig. 11. Comparison of different comprehensive health assessment methods: monotonicity and robustness.

by PCA for PDI_1, PDI_2, PDI_3, and PDI_4, are 0.2986, 0.3205, 0.1957, and 0.1852, respectively, in the generating mode and 0.2815, 0.3256, 0.1874, and 0.2055, respectively, in the pumping mode. Fig. 9 shows the IRC of the 200th, 250th, and 300th operation of the PSU under the generating mode. It can be seen that the degradation degree for each measurement location can be visually shown. Intuitively, the larger the area and perimeter of the quadrilateral, the more severe its corresponding overall degradation. In addition, the IRC can reflect the dynamic changes of each of the PDIs and their different contributions to the comprehensive PDI. For example, we can see that PDI_1 increases the most, while PDI_3 increases the least from the 200th operation to the 300th operation. This result can guide the on-site operation personnel to pay special attention to the health condition of upper X (PDI_1).

Furthermore, the comprehensive PDI of the PSU can be calculated by (9). To illustrate the performance of the proposed IRC in the comprehensive assessment of multiple PDIs of different measurement locations, it is compared with some commonly used multi-indicator evaluation methods, including traditional RC [34], the PCA weighting (PCA-W) method, and the technique for order preference by similarity to an ideal solution (TOPSIS) [35]. PCA-W directly uses the weights calculated by PCA from the historical vibration data to weight and sum the PDIs to obtain the comprehensive evaluation results. The traditional RC and TOPSIS methods can be referred to the literatures [34] and [35], respectively. In addition, to verify the performance of our HCA approach on the whole process, it is compared with LSTMCAE-MGD [20], which was reported as one of the state-of-the-art HCA methods for aircraft engines from multisensor signals. It used MGD to calculate PDIs based on the reconstruction error generated by LSTMCAE. Thus, there are five methods: 1) RC; 2) PCA-W; 3) TOPSIS; 4) LSTMCAE-MGD; and 5) IRC, for comparison in this section. The PDI sequences of these five methods under generating mode are shown in Fig. 10. The aforementioned monotonicity and robustness are used as evaluation metrics. The comparison results are shown in Fig. 11.

From Figs. 10 and 11, we can see that despite using the most advanced deep learning methods, the results of LSTMCAE-MGD are the worst with the smallest monotonicity and robustness. This is because it directly learns the PDI from the vibration signals collected from the four measurement locations, and does not fully consider the multiple influencing factors of the vibration. It also can be seen that among the remaining four methods, TOPSIS is inferior to the other three methods. This may be because objective weighting is not employed in the TOPSIS method. Both PCA-W and IRC use weights obtained from historical vibration data, they are relatively close in terms of robustness indicator. The traditional RC method uses the area of the quadrilateral enclosed by four PDIs as a comprehensive evaluation metric. It also achieves good results in terms of robustness. However, in terms of monotonicity, IRC achieved better results than RC and PCA-W. Moreover, it is impossible for PCA-W to visually and dynamically illustrate the HCA results for PSUs. Although the traditional RC can also visually display the PDIs, it cannot give different importance of PDIs constructed from multisensor data at different locations. The proposed IRC fully utilizes the advantages of both PCA-W and RC, and therefore, achieves the best results.

To sum up, the proposed method achieved excellent performance in all phases of the comparative experiments. The combined results suggest that the proposed HCA method has better engineering application value and practicality. It facilitates the on-site operations and maintenance personnel to understand the health condition of the PSU exactly, and then make rational maintenance plans to prevent potential failures and subsequent losses.

VI. Conclusion and Future Work

This article presented a novel HCA method for PSUs, which focuses on three aspects to overcome the shortcomings of the existing methods as follows.

1) First, an MSM-QRNN-based HBM was proposed, which has the following advantages.
   a) Multiple sensor vibration signals collected from four measurement locations and their seven influencing factors were considered, which is more comprehensive than the existing methods.
   b) MSM can automatically learn the complex interacting relationship between multiple influencing factors.
   c) By using QRNN, the proposed HBM predicts the upper bounds of the health vibration, which can reflect the uncertainty information of the vibration.
2) Second, an FDF was constructed based on the distribution characteristics of historical vibration and warning values specified by the power plant to extract the PDIs for PSUs under the situation lacking "run-to-failure" data.
3) Third, an IRC method was proposed to visually illustrate the health condition of multiple measurement locations and gave an overall HCA for PSUs. The proposed method was applied in a PSU located in Zhejiang Province of China. The comparative experiments showed its outstanding performance.

Moreover, following issues deserves further explorations.

1) This article explored HCA for PSUs under long-term steady-state conditions. However, the degradation information also exists in the transient process of PSUs. It is also worth doing HCA under transient operating conditions.

2) The rms is used to represent the overall vibration level of each operating process. More representative features deserve further study.
3) Due to space limitations, only the HCA of PSUs was performed in this article.

Some specially designed models for health degradation trends prediction should be further investigated.

References

[1] L. Pingkuo and P. Huan, "What drives the green and low-carbon energy transition in China?: An empirical analysis based on a novel framework," *Energy*, vol. 239, 2022, Art. no 122450.

[2] Y. Chen, C. Deng, and Y. Zhao, "Coordination control between excitation and hydraulic system during mode conversion of variable speed pumped storage unit," *IEEE Trans. Power Electron.*, vol. 36, no. 9, pp. 10171–10185, Sep. 2021.

[3] X. An, L. Yang, and L. Pan, "Nonlinear prediction of condition parameter degradation trend for hydropower unit based on radial basis function interpolation and wavelet transform," *Proc. Inst. Mech. Engineers, C: J. Mech. Eng. Sci.*, vol. 229, no. 18, pp. 3515–3525, 2015.

[4] Y. Shan, J. Liu, Y. Xu, and J. Zhou, "A combined multi-objective optimization model for degradation trend prediction of pumped storage unit," *Measurement*, vol. 169, 2021, Art. no. 108373.

[5] W. Zhu *et al.*, "A novel KICA-PCA fault detection model for condition process of hydroelectric generating unit," *Measurement*, vol. 58, pp. 197–206, 2014.

[6] R. B. de Santis and M. A. Costa, "Extended isolation forests for fault detection in small hydroelectric plants," *Sustainability*, vol. 12, no. 16, 2020, Art. no. 6421.

[7] H. Ehya, A. Nysveen, and T. N. Skreien, "Performance evaluation of signal processing tools used for fault detection of hydro-generators operating in noisy environments," *IEEE Trans. Ind. Appl.*, vol. 57, no. 4, pp. 3654–3665, Jul./Aug. 2021.

[8] Y. Lei, N. Li, L. Guo, N. Li, T. Yan, and J. Lin, "Machinery health prognostics: A systematic review from data acquisition to RUL prediction," *Mech. Syst. Signal Process.*, vol. 104, pp. 799–834, 2018.

[9] M. He and W. Guo, "An integrated approach for bearing health indicator and stage division using improved Gaussian mixture model and confidence value," *IEEE Trans. Ind. Informat.*, to be published, doi: 10.1109/TII.2021.3123060.

[10] H. Miao, B. Li, C. Sun, and J. Liu, "Joint learning of degradation assessment and RUL prediction for aeroengines via dual-task deep LSTM networks," *IEEE Trans. Ind. Informat.*, vol. 15, no. 9, pp. 5023–5032, Sep. 2019.

[11] X. Bian, Z. Wei, W. Li, J. Pou, D. U. Sauer, and L. Liu, "State-of-health estimation of lithium-ion batteries by fusing an open circuit voltage model and incremental capacity analysis," *IEEE Trans. Power Electron.*, vol. 37, no. 2, pp. 2226–2236, Feb. 2022.

[12] C. She, Z. Wang, F. Sun, P. Liu, and L. Zhang, "Battery aging assessment for real-world electric buses based on incremental capacity analysis and radial basis function neural network," *IEEE Trans. Ind. Informat.*, vol. 16, no. 5, pp. 3345–3354, May 2020.

[13] Z. Wang, C. Song, L. Zhang, Y. Zhao, P. Liu, and D. G. Dorrell, "A data-driven method for battery charging capacity abnormality diagnosis in electric vehicle applications," *IEEE Trans. Transp. Electrific.*, vol. 8, no. 1, pp. 990–999, Mar. 2022.

[14] P. Wang, R. X. Gao, and W. A. Woyczynski, "Lévy process-based stochastic modeling for machine performance degradation prognosis," *IEEE Trans. Ind. Electron.*, vol. 68, no. 12, pp. 12760–12770, Dec. 2021.

[15] S. Baek and D.-Y. Kim, "Fault prediction via symptom pattern extraction using the discretized state vectors of multisensor signals," *IEEE Trans. Ind. Informat.*, vol. 15, no. 2, pp. 922–931, Feb. 2019.

[16] P. Wen, S. Zhao, S. Chen, and Y. Li, "A generalized remaining useful life prediction method for complex systems based on composite health indicator," *Rel. Eng. Syst. Saf.*, vol. 205, 2021, Art. no. 107241.

[17] T. Yan, D. Wang, M. Zheng, T. Xia, E. Pan, and L. Xi, "Fisher's discriminant ratio based health indicator for locating informative frequency bands for machine performance degradation assessment," *Mech. Syst. Signal Process.*, vol. 162, 2022, Art. no. 108053.

[18] Y. Qin, D. Chen, S. Xiang, and C. Zhu, "Gated dual attention unit neural networks for remaining useful life prediction of rolling bearings," *IEEE Trans. Ind. Informat.*, vol. 17, no. 9, pp. 6438–6447, Sep. 2021.

[19] J. Antoni and P. Borghesani, "A statistical methodology for the design of condition indicators," *Mech. Syst. Signal Process.*, vol. 114, pp. 290–327, 2019.

[20] Z. Ye and J. Yu, "Health condition monitoring of machines based on long short-term memory convolutional autoencoder," *Appl. Soft Comput.*, vol. 107, 2021, Art. no. 107379.

[21] Y. Wei, D. Wu, and J. Terpenny, "Learning the health index of complex systems using dynamic conditional variational autoencoders," *Rel. Eng. Syst. Saf.*, vol. 216, 2021, Art. no. 108004.

[22] L. Guo, Y. Yu, A. Duan, H. Gao, and J. Zhang, "An unsupervised feature learning based health indicator construction method for performance assessment of machines," *Mech. Syst. Signal Process.*, vol. 167, 2022, Art. no. 108573.

[23] X. An, L. Pan, and L. Yang, "Condition parameter degradation assessment and prediction for hydropower units using Shepard surface and ITD," *Trans. Inst. Meas. Control*, vol. 36, no. 8, pp. 1074–1082, 2014.

[24] W. Song *et al.*, "AutoInt: Automatic feature interaction learning via self-attentive neural networks," in *Proc. 28th ACM Int. Conf. Inf. Knowl. Manage.*, 2019, pp. 1161–1170.

[25] A. Vaswani *et al.*, "Attention is all you need," in *Proc. Adv. Neural Inf. Process. Syst.*, 2017, pp. 5998–6008.

[26] W. Zhang, Y. He, and S. Yang, "Day-ahead load probability density forecasting using monotone composite quantile regression neural network and kernel density estimation," *Electric Power Syst. Res.*, vol. 201, 2021, Art. no. 107551.

[27] A. Galassi, M. Lippi, and P. Torroni, "Attention in natural language processing," *IEEE Trans. Neural Netw. Learn. Syst.*, vol. 32, no. 10, pp. 4291–4308, Oct. 2021.

[28] J. W. Taylor, "A quantile regression neural network approach to estimating the conditional density of multiperiod returns," *J. Forecasting*, vol. 19, no. 4, pp. 299–311, 2000.

[29] Y. He and H. Li, "Probability density forecasting of wind power using quantile regression neural network and kernel density estimation," *Energy Convers. Manage.*, vol. 164, pp. 374–384, 2018.

[30] Y. He and Y. Wang, "Short-term wind power prediction based on EEMD-LASSO-QRNN model," *Appl. Soft Comput.*, vol. 105, 2021, Art. no. 107288.

[31] X. An, L. Pan, Z. Gui, and Y. Zhou, "Abnormal condition detection model for pumped storage unit," *Water Resour. Power*, vol. 31, no. 1, pp. 157–160, 2013.

[32] W. Peng, Y. Li, Y. Fang, Y. Wu, and Q. Li, "Radar chart for estimation performance evaluation," *IEEE Access*, vol. 7, pp. 113880–113888, 2019.

[33] M. Sabzekar and S. M. H. Hasheminejad, "Robust regression using support vector regressions," *Chaos, Solitons Fractals*, vol. 144, 2021, Art. no. 110738.

[34] W. Shaojie, H. Liang, J. Lee, and B. Xiangjian, "Evaluating wheel loader operating conditions based on radar chart," *Automat. Construction*, vol. 84, pp. 42–49, 2017.

[35] K. Fang, T. Wang, X. Zhou, Y. Ren, H. Guo, and J. Li, "A TOPSIS-based relocalization algorithm in wireless sensor networks," *IEEE Trans. Ind. Informat.*, vol. 18, no. 2, pp. 1322–1332, Feb. 2022.

Xiaoyuan Zhang received the B.S. and M.S. degrees in thermal energy and power engineering from the North China University of Water Resources and Electric Power, Zhengzhou, China, in 2004 and 2007, respectively, and the Ph.D. degree in hydraulic and hydro-power engineering from the Huazhong University of Science and Technology, Wuhan, China, in 2012.

From 2019 to 2020, he was a Visiting Scholar with the School of Informatics and Computing, Indiana University–Purdue University Indianapolis, IN, USA. He is currently an Associate Professor with the College of Electrical Engineering, Henan University of Technology, Zhengzhou, China. His research interests include power equipment condition monitoring, fault diagnosis, reliability analysis, health management, and the application of intelligent systems.

Yajun Jiang received the B.S. degree in electrical engineering and automation in 2019 from the Henan University of Technology, Zhengzhou, China, where he is currently working toward the M.S. degree in control science and engineering.

His research interests include condition maintenance of hydropower units and automation of power equipment maintenance.

Xian-Bo Wang (Member, IEEE) received the Ph.D. degree in electromechanical engineering from the University of Macau, Zhuhai, Macao, China, in 2018.

He is currently a Lecturer with the College of Electrical Engineering, Henan University of Technology, Zhengzhou, China. His research interests include wind energy generation and conversion, smart grid, Internet of Things, machine learning-based application, data-driven fault diagnosis, modeling and optimal control of complex industrial process, and fault-tolerant control of real-time systems.

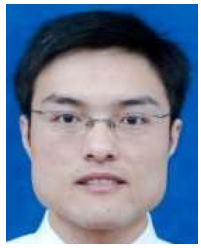

Chaoshun Li (Member, IEEE) received the B.S. degree in thermal energy and power engineering from Wuhan University, Wuhan, China, in 2005, and the Ph.D. degree in water conservancy and hydropower engineering from the Huazhong University of Science and Technology (HUST), Wuhan, China, in 2010.

He is currently a Full Professor with the School of Civil and Hydraulic Engineering, HUST. His research interests include machine learning, intelligent optimization, and control theories and applications.

Jinhao Zhang received the B.S. degree in automation from the Luoyang Institute of Science and Technology, Luoyang, China, in 2020. He is currently working toward the M.S. degree in electronic information with the Henan University of Technology, Zhengzhou, China.

His research interests include mechanical equipment fault diagnosis and signal processing.